Journal of Materials Chemistry

Cite this: *J. Mater. Chem.*, 2012, **22**, 16906

www.rsc.org/materials

PAPER

Versatile fabrication of nanoscale sol–gel bioactive glass particles for efficient bone tissue regeneration

Bo Lei,*[ac] Xiaofeng Chen,*[ab] Xue Han[ab] and Jiaan Zhou[ab]

Received 6th March 2012, Accepted 22nd June 2012
DOI: 10.1039/c2jm31384g

There has been an increased interest in developing nanoscale biomaterials for bone tissue regeneration, due to the biomimetic nano-dimensions and properties compared to natural tissue (bone). Bioactive glass (BG) is regarded as an excellent biomaterial for use in bone regeneration, because of its bioactivity and osteoconductivity. Here, we develop bioactive glass nano-scale particles (NBGs) by sol–gel combining gelation-induced phase separation technology, and demonstrate the effect of bioactive glass dimensions on their physicochemical and biological properties. The micro/nanostructure, surface texture, and bioactive silicon species release were studied to indicate the physicochemical properties of NBGs. The bone-bonding ability was determined by investigating the apatite-forming bioactivity of NBGs. The effect of the micro/nanoscale interface on the attachment and proliferation of human marrow mesenchymal stem cells (hMSCs) was carried out to determine the biocompatibility of NBGs. All samples showed stable silicone release, and the nanoscale particles (40–800 nm) demonstrated a high apatite-forming ability. The biological results showed that all particle dimensions (40–2000 nm) supported hMSCs attachment and proliferation. The NBG with a nanoscale dimension of 40–180 nm significantly enhanced hMSCs proliferation. This study may provide a new route in the design of bioactive biomaterials' nano-interfaces for efficient bone tissue regeneration.

1. Introduction

Since its development in the 1960s, bioactive glass-based (BG) biomaterials have attracted much attention in biomedical applications for bone tissue regeneration, soft tissue restoration, and as drug delivery carriers.[1–3] As compared to other bioceramics, BGs presents many advantages such as biodegradation, high apatite-forming ability, osteoproductivity and angiogenic properties.[4,5] On the other hand, compared with a conventional melting process, the sol–gel technology makes it possible to prepare BGs with various compositions, size and morphology, which is very beneficial for their wider application.[6,7]

Based on the excellent biocompatibility of the natural extracellular matrix (ECM) which possesses a typical nanoscale structure, increased interest has focused on investigating the structure and biological properties of nano-biomaterials such as nano-bioceramics and nanofibrous biopolymers.[8–10] Indeed, a number of studies have shown that nanoscale biomaterials demonstrated enhanced osteoblast attachment, proliferation, differentiation and new bone formation, compared with microscale structures. For example, nanoscale hydroxyapatite (HA) structures have exhibited increased effects on the osteoblasts proliferation and bone formation.[11,12]

Based on the positive results for nanoscale structures, in recent years, much attention has focused on developing nanoscale bioactive glasses (NBG) with controlled size and morphology.[13,14] Although there has been increased interest in fabricating NBG and corresponding nanocomposites, only a limited amount of literature paid attention the biocompatibility and osteogenic inducing ability of NBG.[15,16] Recently, Jones *et al.* investigated the effect of sub-micrometer BG particle concentration on the cellular functions of human mesenchymal stem cells (hMSCs). Their results showed that sub-micrometer particles did not produce any obvious cytotoxicity.[16] Additionally, the nanoscale surface microstructure of sol–gel BG particles has shown enhanced cellular behavior for marrow stem cells.[17,18] Before being used in any application, the physicochemical and biological properties of NBG should be evaluated carefully.

Up to now, almost all the NBG particles reported were prepared by the precipitation of BG sols using alkaline treatment in a basic environment.[19] Due to the multi-compositions of BG (SiO_2–CaO–P_2O_5), it is very difficult to obtain nanoscale particles with a uniform chemical compositions and structure under basic conditions. Secondly, the inhomogeneous structure would result in unstable bioactivity and degradation.[20] Thirdly, the fast gelation of the BG sol usually produced dense colloidal particles which resulted in a low surface texture and reactivity.[21] Because

[a]*School of Materials Science and Engineering, South China University of Technology, Guangzhou 510640, China. E-mail: leiboaray@yahoo.com.cn; Tel: +86-2-940-2848*
[b]*National Engineering Research Center for Tissue Restoration and Reconstruction, Guangzhou 510640, China*
[c]*Department of Dental Laboratory Science and Engineering, Korea University, Seoul 136703, South Korea*

of the poor control of the structure and size of the NBG, it is difficult to compare the physicochemical and biological properties for different NBG particles in reference to size or morphology.

As compared to the base gelation method, acid-catalysis and gelation allows the formation of branched and uniform structures because of the uniform condensation without colloidal particle precipitation.[22] However, acid gelation often results in the formation of a clear BG gel with a continuous network structure, which is going against the formation of NBG particles. On the other hand, our recent studies showed that the formation of separate BG particles was possible if we added a polymer phase into the BG sol.[23–25] The particles formed depends on the microphase separation mechanism between the polymer phase and the BG gel when gelation occurs. For example, we have successfully synthesized porous nanostructures, mesoporous microspheres, and porous microparticles using an acid based gelation co-phase separation technology by adding polyethylene glycol (PEG) and chitosan into the BG sols.[23,24,26] We also prepared monodispersed BG microspheres (BGM) and NBG particles used as bioactive reinforcements for improving the properties of poly (ε-caprolactone) (PCL).[27,28]

Even though there has been increased interest in NBGs, the detailed physicochemical properties, biocompatibility and osteogenic differentiation potential are still unknown. Therefore, in this study, we designed BG particles with different sizes (40–1000 nm) using an acid-catalyzed sol–gel process and gelation-induced phase separation (GIPS) technology. We focused on investigating their physicochemical properties, apatite-forming bioactivity, and biocompatibility. We hypothesised that the nanoscale dimensions of NBGs could induce a positive effect on their physicochemical properties, apatite-forming bioactivity and cellular biocompatibility.

2. Materials and methods

2.1. Synthesis of nanoscale bioactive glass particles

Nanoscale bioactive glass (NBG) particles with a mole composition of 60% SiO_2, 36% CaO, 4% P_2O_5 were synthesized by an acid-catalyzed sol–gel method and gelation-induced phase separation technology. Polyethylene glycol (PEG, $M_w = 10\,000$, Sigma) was chosen as a phase separation agent because of its good solubility in the BG sol. The typical sol–gel process for fabricating BG was performed according to a previous report.[25] Briefly, 20 ml H_2O, 2 ml hydrochloride acid (Guanghua Chemical), 25 g tetraethyl orthosilicate (Sigma), 2.9 g triethyl phosphate (Guanghua Chemical) and 17 g calcium nitrate tetrahydrate (Guanghua Chemical) were mixed in sequence at room temperature. After stirring for 60 min, a given amount of PEG was added into the as formed BG sol. After another 60 min, the resulting BG sol was sealed in plastic tubes and placed in an oven at 60 °C for gelation and phase separation. Next, the white gel particles were washed twice with absolute ethanol, followed by freeze drying for 24 h. Finally, to obtain pure NBG particles, the dried powder was sintered at 600 °C (5 °C min^{-1}) for 2 h. In this study, the amount of PEG determined the degree of phase separation and the NBG size. Therefore, PEG/TEOS weight ratios of 10 wt%, 15 wt% and 20 wt% were used and the corresponding NBG were denoted P1-NBG, P2-NBG, P3-NBG respectively.

2.2. Morphology, structure and composites evaluation

The particles' morphology was examined using field emission scanning electron microscopy (FE-SEM) (JSM6330F, JEOL, Japan). For FE-SEM observations, the NBG particles were sputter-coated with gold for 150 s under a gas pressure of 40 mTorr and then imaged. The elemental compositions and distribution maps were recorded by energy dispersive spectroscopy (EDS, OXFORD). The crystalline phase composition of samples was identified by powder X-ray diffraction (XRD, X'Pert PRO, PANalytical) with Cu K_α radiation (wavelength 1.548 Å). The specific surface area, pore volume and pore size of NBG were determined by Brunauer–Emmett–Teller (BET) and Barret–Joyner–Halenda (BJH) analyses (Tristar3000, Micromeritics, USA). The particle size distributions of NBG were tested by counting at least 100 particles based on the SEM images using software image-Pro Plus 6.0 (Media Cybernetics, Inc. USA).

2.3. Biodegradation and Si species release characterization

The degradation and Si species release behavior of the NBGs were analyzed by soaking them in simulated body fluid (SBF) for several days. The SBF composition and preparation was in accordance with previous reports.[29] The soaking concentrations of particles in SBF solution was set as 1 mg ml^{-1}. At every time point, 5 ml clear solution was removed and replaced by the same amount of fresh SBF. The Si concentration was determined by inductively coupled plasma atomic emission spectrophotometry (ICP-AES, PS1000-AT, Leeman, USA). To obtain the mean value and standard error, three species for every sample were tested at each time.

2.4. Apatite-forming bioactivity assessment

The SBF with a pH value of 7.35 was used to test the *in vitro* apatite-forming ability of NBG. The test procedure was similar to that in our previous report.[20] The formation, morphology and structure of apatite layers on the surfaces of NBG were determined by FE-SEM, XRD and Fourier Transform Infrared Spectroscopy (FTIR, Nicolet 6700, Thermo Sci., USA).

2.5. Isolation and culture of human marrow mesenchymal cells (hMSCs)

The standard Ficoll–Hypaque (FH) density gradient centrifugation technology was used to isolate hMSCs from the iliac crest of healthy human volunteers with a mean age of 22 years.[30] This isolation was in accordance with the ethical guidelines of South China University of Technology (SCUT). Typically, after centrifuging the marrow in an FH solution (TBD Biotech, Tianjin), the obtained mononuclear cells were washed and resuspended in Dulbecco's Modified Eagle Medium (DMEM) supplemented with 10 vol.% fetal bovine serum (FBS), 1% v/v antibiotics (Invitrogen, UK) (complete culture media). The medium was changed every the other day. After culturing in the medium for 2–3 weeks, the cell monolayer was denoted as

passage 0. Then the cells were cultured by passage and the fifth passage (P5) was used for all the experiments.

2.6. Fabrication of NBG interface for cells culture

To investigate the hMSCs attachment and growth behavior on the NBG particles' interface, the NBG particles were sputtering-coated on the surface of cleaned glass slides (Dingjie Biotech., China). The NBG interface was prepared according to a previous report.[20] The blank glass without NBG particles was also prepared for comparison.

2.7. Cells culture on NBG particles

To pre-wet the particles, the sterilized samples were soaking in 2 ml culture medium for 5 hours. Then the medium was removed and hMSCs were seeded on the samples in the 24 well plate at a density of 2×10^4 cells per ml complete culture medium. The culture plate was incubated at 37 °C with 5% CO_2 for 2 h to allow the cells to attach, followed by adding 1 ml complete culture medium in every well. The samples with cells were cultured for 4 h, 1 day, 3 days, 7 days according to different evaluation projects. The culture medium was changed every the other day. The culture medium may be different depending on the investigating items.

2.8. Attachment and proliferation evaluation of hMSCs

The attachment morphology of hMSCs on the surface of NBG was tested after culturing for 4 hours, and qualitatively monitored by environmental scanning electric microscopy (ESEM, Quanta200, FEI, the Netherlands) and fluorescence microscopy (FM, 40FLAxioskop, Zeiss, Germany). For the ESEM observations, hMSCs were fixed by 2.5% glutaraldehyde for 30 min and dehydrated for 5 min using gradient ethanol concentrations (20%, 50%, 70%, 90% and 100% v/v in water). After drying at a room temperature, the samples were coated with gold for 100 seconds under a gas pressure of 35 mTorr and observed by ESEM. For the FM assessment, hMSCs were stained using a live cells labeling kit (Cell Explorer, AAT Bioquest). The staining process was according to the kit instructions. In brief, at the time point, the culture medium was replaced by the staining solution, incubated at 37 °C for 1 h, followed by washing with phosphate buffer solution (PBS) and then observed by FM.

The attachment ability of cells at 4 hours was quantitatively evaluated by 3-(4,5-dimethylthiazol-2-yl)-2,5-diphenyl tetrazolium bromide (MTT) colorimetric method (Amresco, USA).[20] Briefly, at the time point, samples were washed with PBS, followed by incubation with 0.5 ml of 0.5 mg ml^{-1} of MTT solution for 4 h at 37 °C. Then the absorbance value of the solution after reaction was determined at 490 nm by a microplate reader (Thermo 3001, Thermo). Four specimens per sample were tested and each test was performed in triplicate.

The proliferation of hMSCs was carried out by testing live cell fluorescence morphology and viability after culturing for 1, 3, 7 days. The hMSCs fluorescence morphology was evaluated by cell staining and the cell viability was tested by the MTT method, as described above. Four specimens for every sample were analyzed and each test was performed in triplicate.

2.9. Statistical analysis

Data for all experiment were expressed as mean ± standard deviation (SD) and the differences were analyzed using Student's *t*-test. The significant differences were considered at a P value less than 0.05.

3. Results

3.1. Synthesis and structural characterizations of NBGs

To investigate the effects of particle morphology and size on the properties of bioactive glasses (BG), nanoscale bioactive glass particles (NBGs) were first developed through a sol–gel process and gelation-induced phase separation (GIPS) technology. Polyethylene glycol (PEG) as a phase separation agent was introduced into the BG sol. Fig. 1 shows the preparation process of NBGs. NBG particles of different sizes were fabricated by controlling the concentration of PEG in the BG sols (Fig. 1A). The gelation of the BG sol was induced by aging at 60 °C in a sealed environment (Fig. 1B). By adjusting the PEG/tetraethoxysilane (TEOS) weight percent to 10%, 15%, and 20%, the particle diameter distributions of NBG were 2000–4000 nm (P1-NBG), 400–800 nm (P2-NBG) and 40–180 nm (P3-NBG) respectively (Fig. 1C and D). The addition of PEG produces spherical NBG particles morphology with a slight aggregation (Fig. 1C).

The change in particle size could result in the variation of the materials surface properties. As shown in Table 1, the specific surface area (SSA) and total pore volume (TPV) significantly increased with decreasing NBG particles size. For example, P3-NBG possessed significantly higher SSA (86 $m^2\ g^{-1}$) and TPV (0.26 $cm^3\ g^{-1}$), compared with those of P1-NBG (2 $m^2\ g^{-1}$ and 0.02 $cm^3\ g^{-1}$). Fig. 2 shows the crystalline phase structure, chemical composition and element distributions (Si, Ca) of the NGBs. All the NBGs prepared in this study displayed the representative amorphous feature with a wide peak between 20° and 35° (Fig. 2a). Moreover, the diffraction peak for P3-NBG was wider than that for P1-NBG. Chemical composition analysis indicated the presence of Si, Ca, P, O in the NBG structure, as shown in Fig. 2b. The element maps demonstrated the uniform distributions of Si (Fig. 2c) and Ca (Fig. 2d) in the NBGs. The results above demonstrated that NBG particles with controlled size and uniform structure were fabricated successfully.

3.2. Biodegradation and Si species release behavior of NBGs

The effect of the particle sizes on the degradation and Si species release behavior of NBG were evaluated by soaking the samples in simulated body fluid (SBF). Fig. 3 shows the results of biodegradation and Si release during the 7 day soaking period. The Si concentration released from the NBG increased quickly in the first 48 hours and remained stable in after a longer soaking time. The figure inset indicates that the Si release concentration significantly increased as the particle size decreased, during the initial 24 hours. In the other words, decreasing the particle size can significantly enhance the BG degradation and Si release ability by increasing the surface area of particles.

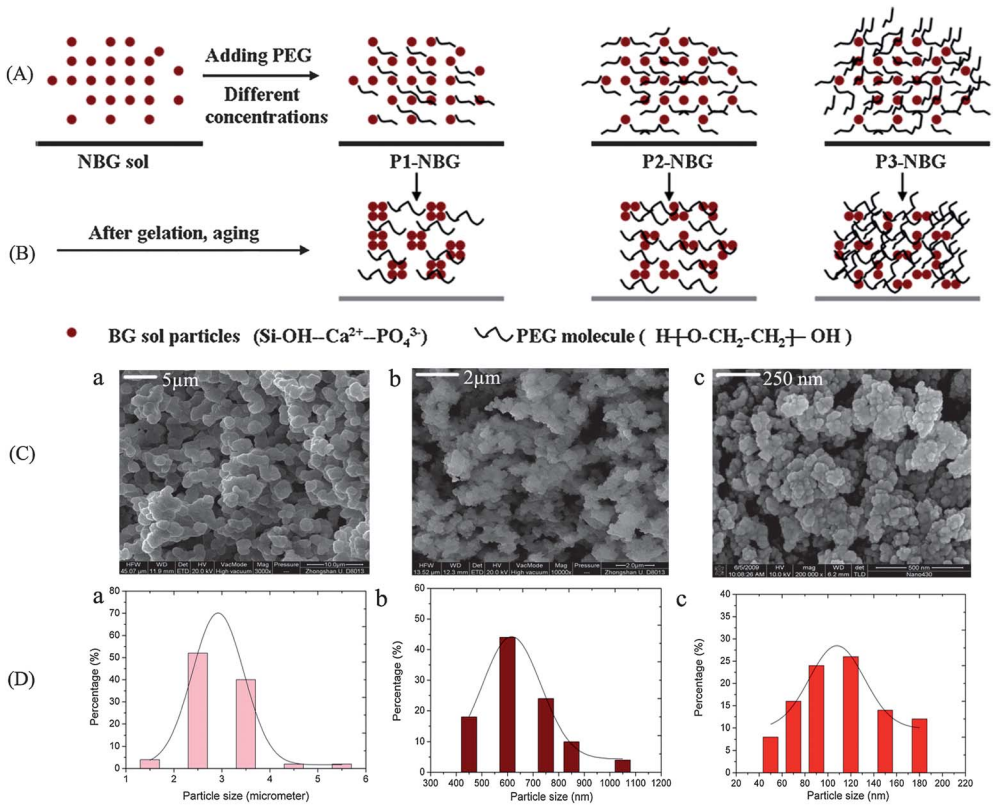

Fig. 1 Fabrication diagram and structure characterization of NBGs using acid-based sol–gel and gelation-induced phase separation technology. (A) NBGs particle size was controlled by introducing different PEG concentrations into the BG sols; (B) phase separation between PEG molecules and BG sol particles was induced by aging at 60 °C; (C) SEM images showing particle morphology of P1-NBG (a), P2-NBG (b) and P3-NBG (c); (D) nanoscale particles size statistics (more than 100) of P1-NBG (a), P2-NBG (b) and P3-NBG (c). Scale bars are indicated on images.

3.3. *In vitro* apatite-forming bioactivity of NBGs

For bone tissue regeneration biomaterials, apatite-forming bioactivity *in vitro* is very important because this property has shown positive relevance with the bone-forming activity *in vivo*.[31] Therefore, in this paper, the apatite-forming bioactivity of NBGs of different sizes was investigated by soaking samples in SBF for 36 hours. The surface morphology, chemical structure and crystalline phase composition of the apatite layer formed on the NBGs are shown in Fig. 4.

As compared to the surface morphology before soaking, a new apatite layer was formed on the surfaces of all the samples (P1-NBG, P2-NBG, P3-NBG), as shown in Fig. 4a–c. However, the morphology and size of apatite layer formed on the NBGs were a little different from each other. Sub-micrometer (300–400 nm) and particle-like apatite was found on the surface of P1-NBG (Fig. 4a). Nanoscale (80–150 nm) and rod-like apatite was formed on the surface of P2-NBG (Fig. 4b). P3-NBG induced the formation of needle and flake-like apatite layers (50–150 nm) (Fig. 4c).

The crystalline structure of the apatite layer precipitated on the surface of the NBGs after immersing in SBF was identified by XRD analysis, as shown in Fig. 4d. By comparing with the XRD patterns before soaking (Fig. 2a), the new characteristic peaks at $2\theta = 26°$ (002), 32° (211), 39°(310), 46° (222), 49° (213), 53° (004) were assigned to a hydroxyapatite (HA) phase (JCPDS 09-0432). That means that all the samples (P1-NBG, P2-NBG, P3-NBG) could induce the formation of HA with poor crystallinity after soaking in SBF for 36 hours. In addition, the XRD peaks intensities for the HA phase increased with a decrease in particles sizes (from P1-NBG to P3-NBG), which demonstrated a fast HA-forming bioactivity for the nanoscale BG particles (40–800 nm).

The FT-IR analysis was further used to confirm the chemical structure of HA formed on the surface of NBGs, as shown in Fig. 4e. Before soaking (data not shown), the FTIR spectrum of NBG exhibited the representative characteristic absorption

Table 1 Structure and properties summary of NBGs

Samples	Particles size (nm)	Specific surface area ($m^2\ g^{-1}$)	Total pore volume ($cm^3\ g^{-1}$)	Pore size (nm)
P1-NBG	2000–4000	2	0.02	Below 2 nm
P2-NBG	400–800	20	0.08	18
P3-NBG	40–180	86	0.26	10

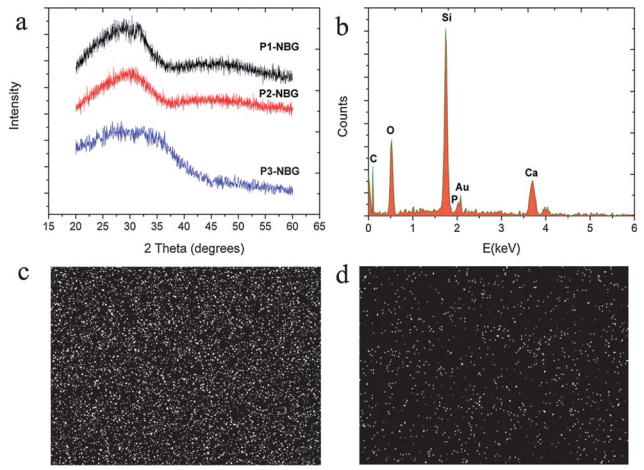

Fig. 2 Structure and compositions of NBGs. (a) XRD patterns showing the crystalline structure of the nanoparticles; (b) EDS analysis showing the element composition of P3-NBG; (c and d) element maps showing the Si (c) and Ca (d) distributions in the structure of P3-NBG.

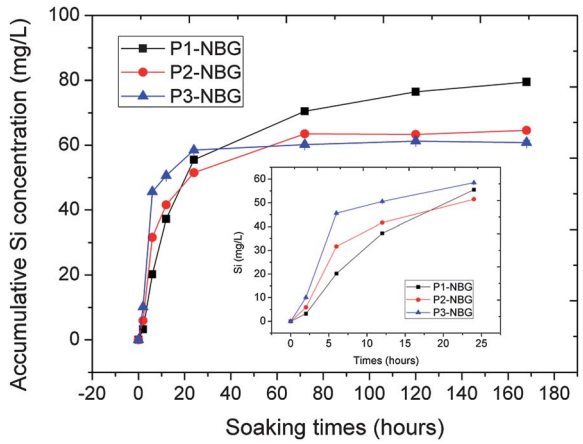

Fig. 3 *In vitro* biodegradation and bioactive Si species release behavior of NBGs during 7 days of SBF soaking. The figure inset shows the Si release profiles for the first 24 hours in SBF, which indicates the difference in degradation ability for the NBGs. The results represent a mean and standard deviation (SD) for every sample ($n = 3$).

bands of Si–O–Si bonds at 1060 cm^{-1} (stretch vibration), 798 cm^{-1} (bending vibration), and 480 cm^{-1} (bending vibration).[7] However, after soaking in SBF, the new bands appeared at 562 cm^{-1}, 603 cm^{-1}, 962 cm^{-1} and 1026 cm^{-1}, and were assigned to P–O vibrations of PO_4^{-3} tetrahedra in the HA structure. The band between 3300 and 3600 cm^{-1} was attributed to the vibration from hydroxyls (OH) in HA. In addition, the bands at 873 cm^{-1}, 1430 cm^{-1} and 1480 cm^{-1} were characteristics of carbonate (CO_3^{2-}). The presence of PO_4^{3-}, OH and CO_3^{2-} indicated that the formed HA on NBGs was carbonated HA (CHA).[32] The vibration band intensity for HA increased with the decrease of NBG particles size, which was in accordance with the results from XRD analysis. It should be emphasized that P3-NBG (40–180 nm) could induce CHA precipitation with better crystallinity and chemical structure, as compared to P2-NBG and P3-NBG (400–4000 nm).

3.4. Attachment and proliferation of hMSCs on NBGs

Although nanoscale biomaterials displayed unique physicochemical properties and bioactivity, their biological safety is of concern when considering them as tissue regeneration materials *in vivo*. Therefore, the biocompatibility of NBG particles should be analyzed before further molecular biology testing. In this study, the biocompatibility and cytotoxicity of the NBG particles were evaluated by testing the attachment and proliferation of hMSCs on the surface of the nanoparticles.

Fig. 5 shows the attachment ability of hMSCs on the surfaces of P1-NBG (Fig. 5a and e), P2-NBG (Fig. 5b and f), and P3-NBG (Fig. 5c and g) in a short culture time (4 h). All the NBGs could induce hMSCs adherence and spread (a–c). In addition, compared with P1-NBG and P2-NBG, the cells displayed a better attachment and spread on the surface of P3-NBG. The fluorescent images (e–g) indicate that hMSCs showed a spread morphology and good viability on all samples. The quantitative 3-(4,5-dimethylthiazol-2-yl)-2,5-diphenyl tetrazolium bromide (MTT) test also showed that the cells viability has no significant difference among various NBGs, as shown in Fig. 5d.

The proliferation ability of hMSCs on the surfaces of P1-NBG, P2-NBG and P3-NBG was determined by fluorescent microscopy and MTT evaluation after culturing for 1, 3 and 7 days, as shown in Fig. 6 and 7. During the 7 days culture period, cells displayed regular proliferation ability on all NBGs. After 3 days, hMSCs showed a multi-layer structure on P3-NBG (Fig. 6F) and a mono-layer morphology on P1-NBG (Fig. 6D). However, at the same time point (3 days), the cells demonstrated a low density and an aggregated morphology on the surface of P2-NBG (Fig. 6E). After 7 days, hMSCs displayed a multi-layer distribution on all NBG surfaces (Fig. 6G, H and I). In addition, many mineralized particles were present in the cellular matrix (Fig. 6G, H and I). Quantitative MTT tests demonstrated that P1-NBG and P3-NBG showed significantly higher cell proliferation than P2-NBG at a culture time of 3 days (Fig. 7). Up to 7 days, hMSCs exhibited a significant slightly higher viability on P2-NBG, as compared to P1-NBG and P2-NBG.

4. Discussions

Microscale and nanoscale biomaterials have been paid a large amount of attention in biomedical applications because of their features mimicking the extracellular matrix (ECM).[8] In recent years, nanoscale bioactive glass (NBG) has been fabricated using physical methods or chemical precipitation technology for bone tissue regeneration.[14,15] However, because of the uncontrolled synthesis of NBGs (especially in the particle structure and size), the detailed correlations between NBG structures, physicochemical properties and biocompatibility have not understood yet.

In this paper, we demonstrated that NBGs with different structure and size could be successfully synthesized by an acid-catalyzed sol–gel process and gelation-induced phase separation technology. This process allows the control of the BG particle size by variation of the phase separation agent concentrations in the sol. During *in situ* gelation, the BG phase and PEG phase separated, and this produced the tailored particles size after removing PEG by sintering. The NBG surface properties, such as specific surface area and pore volume, increased with

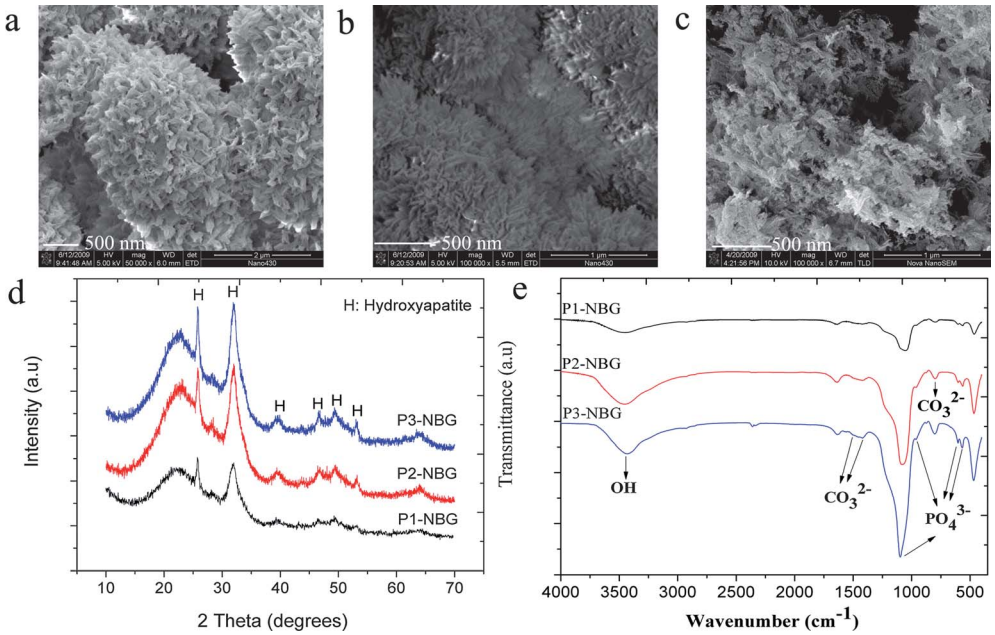

Fig. 4 The *in vitro* apatite-forming bioactivity of NBGs in SBF. (a–c) SEM images showing the surface morphology of P1-NBG (a), P2-NBG (b), P3-NBG (c) after soaking in SBF for 36 h; (c) XRD patterns indicating the phase composition change of the NBGs after soaking for 36 h; (d) FT-IR analysis exhibiting the surface chemical structure of samples after soaking for 36 h. The scale bars and characteristic peaks (bands) are shown in the figure.

decreasing particle size (Table 1). P1-NBG presented a negligible specific surface area, pore volume and pore size, which could be explained by the PEG coating mechanism. For micrometer particles (P1-NBG), the presence of the PEG coating prevented the BG particles sintering, which resulted in relatively dense particles (small specific surface area). The significant improvement in specific surface area for P2-NBG and P3-NBG was due to the decrease of particle size and typical nano-effects. The mesopores presented in the structure of P2-NBG and P3-NBG, were assigned to pores between particles according to the N_2 absorption–desorption isothermal curves (data not shown). The detailed formation mechanism of NBG will be studied in the future.

For bone tissue regeneration, biodegradation and bioactive Si species release are the main features and advantages of BG materials, which can activate osteogenic gene expression.[1] In our study, in the first soaking of 24 hours, it was easy to understand that Si release speed increased with decreasing NBG particles size (P3-NBG) (Fig. 3). Because P1-NBG, P2-NBG, P3-NBG presented the same phase structure and composition (Fig. 2), their degradation was dependent on the particle size and surface properties of BG. A small particles size and high specific surface area would enhance BG contact surface area with SBF, which increased the biodegradation of BG. On the other had, the relatively stable Si release was achieved for all NBGs during 7 days of soaking, which benefited from their less-porous particle structure.

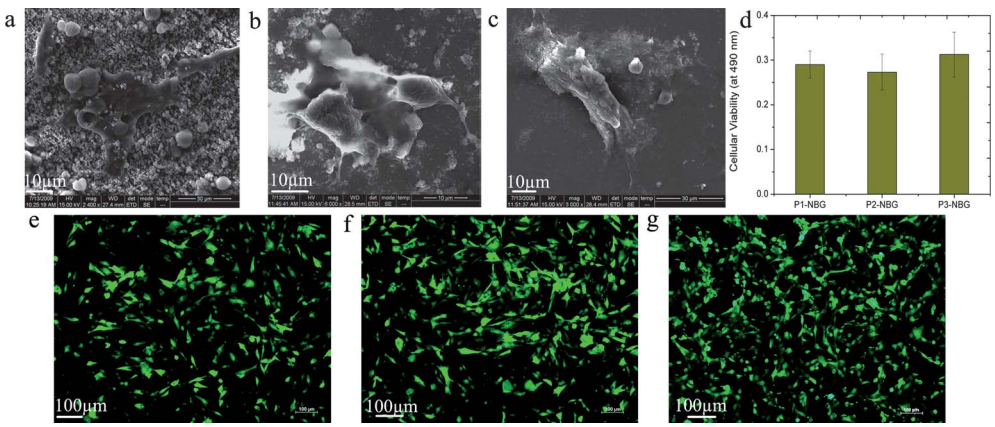

Fig. 5 HMSCs attachment morphology and viability after culturing on NBGs for 4 hours. (a–c) SEM images showing the cell morphology on the surface of P1-NBG (a), P2-NBG (b), P3-NBG (c); (d) MTT evaluation indicating the cells viability, the result represents the mean and SD ($n = 4$), differences between the values were not statistically significant ($p > 0.05$); (e–g) FM images exhibiting the live cells viability and morphology by staining using live cell labeling kit. Scale bars are shown on images.

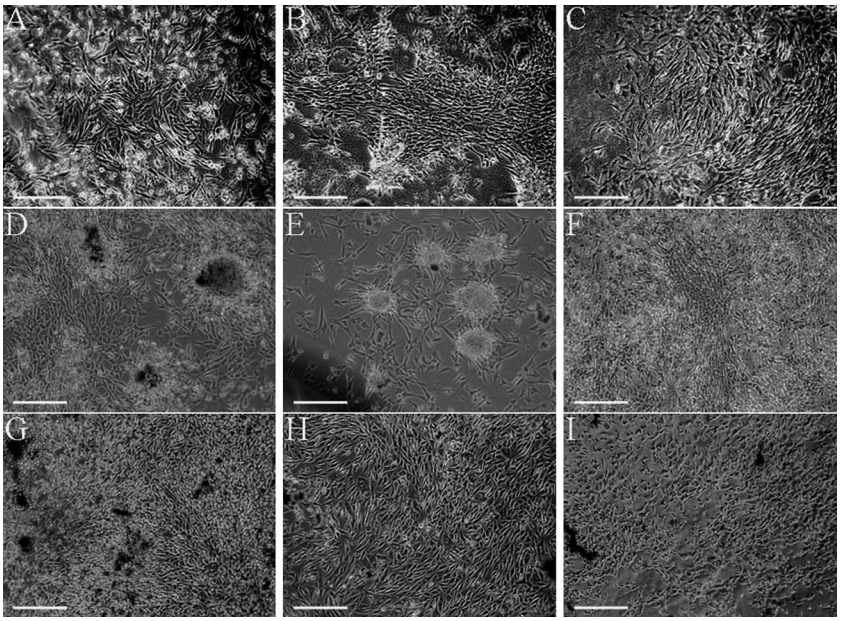

Fig. 6 Qualitative analysis for the proliferation of hMSCs on the NBGs surfaces after different culture periods. (A, D and G) FM images of cells after being cultured on P1-NBG for 1 day (A), 3 days (D) and 7 days (G); (B, E and H) FM images of cells after being cultured on P2-NBG for 1 day (B), 3 days (E) and 7 days (H); (C, F and I) FM images of cells after being cultured on P3-NBG for 1 day (C), 3 days (F) and 7 days (I); scale bar on images means 200 μm.

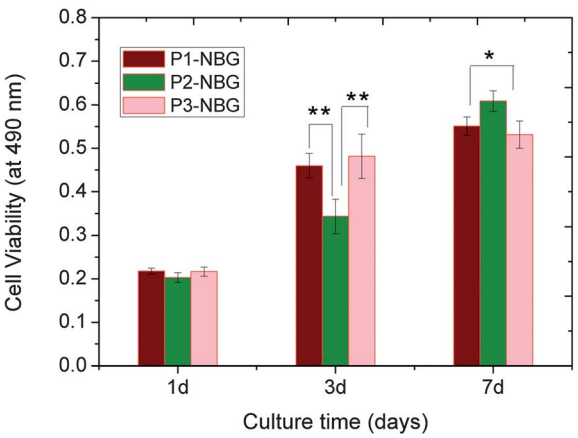

Fig. 7 Quantitative hMSCs proliferation after different culturing periods on NBGs, the results represent the mean and SD ($n = 4$), differences between the values were statistically significant when $*p < 0.05$, $**p < 0.01$.

Good apatite-forming bioactivity *in vitro* is the other advantage of BGs. According to the bioactivity mechanism of BG, the surface properties, crystalline phase structure, and degradation in body fluid should be responsible for their apatite-forming bioactivity.[1,4,5,17] It is well recognized that high specific surface area and pore volume would provide more nucleation centers for apatite formation.[18] This can explain why P2-NBG and P3-NBG showed higher apatite-forming abilities than P1-NBG (Fig. 4). On the other hand, in addition to the environment conditions (pH, ion concentrations *et al.*), the morphology of apatite formed by biomineralization is controlled by the substrate's structure and morphology.[33] In the process of bone tissue mineralization, the nucleation and growth of apatite is dependent on the collagen fiber size and structure which determine the morphology and size of the apatite.[33] In our study, P1-NBG, P2-NBG, P3-NBG had the same crystallinity and chemical composition, and only showed different particles size. We believe that the morphological and dimensional differences of the apatite formed on the NBGs were due to the BG particles size. For example, the needle and flake-like apatite formed on P3-NBG was attributed to BG particle size (40–180 nm), pores (12 nm) and fast nucleation kinetics.

Nanoscale bioactive glasses have previously, and in this study, shown improved surface properties and apatite-forming bioactivity.[7,18,23] Even so, the biocompatibility of BG nanoparticles is still of concern for their application in tissue regeneration. However, few studies focus on investigating the cellular biocompatibility of BG nanoparticles, mostly this may be because of the uncontrolled particles sizes achieved using general fabrication methods. Previous studies demonstrated that sub-micrometer BG particles (200–250 nm) with high silica content (85% SiO_2) did not produce any cytotoxicity for hMSCs in a suitable concentration.[16] Another study showed that bioactive glass nanoparticles could induce cementoblast proliferation.[15] In our study, NBGs with different sizes support the attachment and proliferation of hMSCs, which demonstrated the cellular biocompatibility of nanoscale BG particles.

The different hMSC responses (attachment and proliferation) to P1-NBG, P2-NBG, P3-NBG could be attributed to the BGs physical structure (surface textures and nanotopography), chemical properties (bioactive silicon release) and apatite-forming ability. It is well known that the surface properties (topography, roughness and surface area) of biomaterials have a great

effect on cell attachment.[34] High specific surface area been has shown to enhance protein and growth factor adsorption, which are beneficial for subsequent cell adherence.[35] This evidence should be the cause of the better attachment morphology of hMSCs on P3-NBG and P2-NBG as these have higher specific surface area and pore volume than P1-NBG. However, the cell proliferation was significantly lower on P2-NBG after 3 days compared with P1-NBG and P3-NBG. After 7 days, hMSCs on P2-NBG showed a significantly higher viability than the other NBGs. These proliferation results can not be simply explained by the different surface properties of the NBGs, but depend on their ions production release and apatite-formation ability . In the past decades, studies on BG have shown that bioactive Si release and apatite formation are critical for bone-related cell proliferation and differentiation.[35,36] Bioactive Si concentrations in media between 10 and 30 mg l^{-1} have shown enhanced proliferation and differentiation for osteoblasts.[37] On the other hand, fast biological apatite formation on bioactive glass could efficiently stabilize Si release, which was also helpful for cell proliferation.[20] Thirdly, high sub-micrometer BG particle concentration has been shown to decrease hMSCs proliferation.[16] In our study, P1-NBG presented a slow Si release and P3-NBG showed fast biological hydroxyapatite formation, which contributed to the hMSCs proliferation. The decreased cell proliferation could be attributed to the activation of hMSCs differentiation.[38]

5. Conclusions

Our results indicate that NBG particles size and surfaces can be controlled successfully by acid-catalyzed sol–gel process and gelation-induced polymer phase separation technology. Depending on the nanoparticle's dimensions and surface texture, the NBGs presented stable tailored Si release behavior and biological apatite formation. Sub-micrometer and nanometer NBGs showed high hydroxyapatite-forming bioactivity and Si release. NBGs surfaces support hMSC attachment and proliferation initially, showing the good biocompatibility of NBGs. Micrometer and nanometer NBGs enhanced hMSCs proliferation compared with sub-micrometer particles. The improved biological properties of NBGs could be attributed to the combined effects of nanotopography, Si release and biological apatite formation. Investigating the detailed effect of NBGs on hMSC growth and differentiation behavior is in progress. We believe that this study will motivate the development and applications of bioactive nano-biomaterials in bone tissue regeneration and stem cell-based therapy.

Acknowledgements

This study was supported by National Natural Science Foundation of China (Grant no. 51072055), the key project of the National Natural Science Foundation of China (Grant no. 50830101) and the National 973 project of China (2011CB606204).

References

1 L. L. Hench and J. M. Polak, *Science*, 2002, **295**, 1014.
2 R. M. Day, A. R. Boccaccini, S. Shurey, J. A. Roether, A. Forbes and L. L. Hench, *Biomaterials*, 2004, **25**, 5857.
3 Z. R. Domingues, M. E. Cortes, T. A. Gomes, H. F. Diniz, C. S. Freitas, J. B. Gomes, A. M. Faria and R. D. Sinisterra, *Biomaterials*, 2004, **25**, 327.
4 L. L. Hench, *J. Mater. Sci.: Mater. Med.*, 2006, **17**, 967.
5 A. A. Gorustovich, J. A. Roether and A. R. Boccaccini, *Tissue Eng., Part B: Rev.*, 2010, **16**, 199.
6 R. Li and L. L. Hench, *J. Appl. Biomater.*, 1991, **2**, 231.
7 X. Chen, B. Lei, N. Zhao and Y. Wang, *J. Non-Cryst. Solids*, 2009, **355**, 791.
8 K. Kim and J. P. Fisher, *J. Drug Targeting*, 2007, **15**, 241.
9 V. Mailänder and K. Landfester, *Biomacromolecules*, 2009, **10**, 2379.
10 J. M. Holzwarth and P. X. Ma, *Biomaterials*, 2011, **32**, 9622.
11 Z. Shi, X. Huang, Y. Cai, R. Tang and D. Yang, *Acta Biomater.*, 2009, **5**(1), 338–345.
12 L. Meirelles, A. Arvidsson, M. Andersson, P. Kjellin, T. Albrektsson and A. Wennerberg, *J. Biomed. Mater. Res., Part A*, 2008, **87A**, 299.
13 B. Lei, X. Chen, Y. Wang and N. Zhao, *Mater. Lett.*, 2009, **63**, 1719.
14 Z. Hong, R. L. Reis and J. F. Mano, *J. Biomed. Mater. Res., Part A*, 2009, **88A**, 304.
15 S. M. Carvalho, A. A. R. Oliveira, C. A. Jardim, C. B. S. Melo, D. A. Gomes, M. F. Leite and M. M. Pereira, *J. Tissue Eng. Regener. Med.*, 2011, DOI: 10.1002/term.488.
16 S. L. Labbaf, O. Tsigkou, K. H. Müller, M. M. Stevens, A. E. Porter and J. R. Jones, *Biomaterials*, 2011, **32**, 1010.
17 B. Lei, X. Chen, Y. Wang, N. Zhao, C. Du and L. Fang, *Biomed. Mater.*, 2010, **5**, 054103.
18 B. Lei, X. Chen, Y. Wang, N. Zhao, C. Du and L. Fang, *J. Biomed. Mater. Res., Part A*, 2010, **94A**, 1091.
19 A. R. Boccaccini, M. Erol, W. J. Stark, D. Mohn, Z. Hong and J. F. Mano, *Compos. Sci. Technol.*, 2010, **70**, 1764.
20 B. Lei, X. Chen, X. Han and Z. Li, *J. Mater. Chem.*, 2011, **21**, 12725.
21 L. L. Hench and J. K. West, *Chem. Rev.*, 1990, **90**, 33.
22 C. J. Brinker and G. W. Scherer, *Sol–gel Science*, Academic Press, New York, 1989.
23 B. Lei, X. Chen, Y. Wang, N. Zhao, C. Du and L. Fang, *J. Non-Cryst. Solids*, 2009, **355**, 2678.
24 B. Lei, X. Chen, Y. Wang, N. Zhao, C. G. Miao, Z. Li and C. Lin, *Mater. Lett.*, 2010, **64**, 2293.
25 B. Lei, X. Chen and Y. H. Koh, *J. Sol-Gel Sci. Technol.*, 2011, **58**, 656.
26 B. Lei, K. H. Shin, Y. W. Moon, D. Y. Noh, Y. H. Koh, Y. Jin and H. E. Kim, *J. Am. Ceram. Soc.*, 2012, **95**, 30.
27 B. Lei, K. H. Shin, D. Y. Noh, Y. H. Koh, W. Y. Choi and H. E. Kim, *J. Biomed. Mater. Res., Part B*, 2012, **100B**, 967.
28 B. Lei, K. H. Shin, I. H. Jo, Y. H. Koh, W. Y. Choi and H. E. Kim, *Biomed. Mater.*, 2012, submitting.
29 B. Lei, X. Chen, Y. Wang, N. Zhao, C. Du and L. Fang, *J. Non-Cryst. Solids*, 2009, **355**, 2583.
30 M. F. Pittenger, A. M. Mackay, S. C. Beck, R. K. Jaiswal and R. Douglas, *Science*, 1999, **284**, 143.
31 T. Kokubo and H. Takadama, *Biomaterials*, 2006, **27**, 2907.
32 B. Lei, X. Chen, Y. Wang, N. Zhao, C. Du and L. Fang, *J. Am. Ceram. Soc.*, 2010, **93**, 32.
33 F. Nudelman, K. Pieterse, A. George, P. H. H. Bomans, H. Friedrich, L. J. Brylka and P. A. J. Hilbers, *Nat. Mater.*, 2010, **9**, 1004.
34 S. A. Catledge, Y. K. Vohra, S. L. Bellis and A. A. Sawyer, *J. Nanosci. Nanotechnol.*, 2004, **4**, 986.
35 P. Ducheyne and Q. Qiu, *Biomaterials*, 1999, **20**, 2287.
36 A. Hoppe, N. S. Guldal and A. R. Boccaccini, *Biomaterials*, 2011, **32**, 2757.
37 O. Tsigkou, Effects of Bioactive Resorbable Materials on Human Primary Osteoblasts: Investigating the Role of Bioglass on Osteogenesis, PhD thesis, Imperial College London, 2006.
38 R. O. Navarrete, S. L. Hyzy, D. L. Hutton, C. P. Erdman, M. Wieland, B. D. Boyan and Z. Schwartz, *Biomaterials*, 2010, **31**, 2728.